Spectral and electron-collision properties of atomic ions. II. Inner-shell properties

Steven T. Manson
Department of Physics and Astronomy, Georgia State University, Atlanta, Georgia 30303

Constantine E. Theodosiou
Department of Physics and Astronomy, The University of Toledo, Toledo, Ohio 43606

Mitio Inokuti
Argonne National Laboratory, Argonne, Illinois 60439
(Received 26 November 1990)

In this report, a follow-up to our earlier paper [Theodosiou, Manson, and Inokuti, Phys. Rev. A **34**, 943 (1986)] on comprehensive calculations of various properties of all atomic ions in all stages of ionization with nuclear charge $Z \leq 50$, we investigate, within the Hartree-Slater approximation, inner-shell properties including orbital binding energies, x-ray transition energies and rates, photoionization cross sections, and expectation values of powers of electron radial coordinates. Throughout we concentrate on enumerating general trends of the properties as functions of the nuclear charge Z and the total electron number N. The systematics thus found for highly stripped ions (i.e., for ions in which $Z-N$ is appreciable) are interpreted in terms of the outer-shell screening and the hydrogenic shell structure in which complete shells occur at $N=n(n+1)(2n+1)/3 = 2, 10, 28, 60, \ldots$, for principal quantum numbers $n = 1, 2, 3, 4, \ldots$, respectively.

I. INTRODUCTION

The laboratory study of the properties of multicharged positive atomic ions is demanding because of special conditions such as the high temperatures necessary to produce these ions in quantity. Nevertheless, ions abound in astrophysical and fusion plasma environments, among others. To learn something of their properties, given the scarcity of experimental results, theory is required.

In previous work[1,2] the asymptotic quantum defects for ions with atomic number $Z \leq 50$ were studied, giving basic information about discrete excited states and low-lying continuum states of atomic ions. Data were generated by using the Hartree-Slater central-field model[3-5] and were investigated by using each of three alternative pictures: the isoelectronic, where the electron number N is held constant; the isonuclear, where the atomic number Z is held constant; and the isoionic, where the ionicity $Z-N$ or the order of the spectrum $z=Z-N+1$ is held constant. Each of these pictures shows different aspects of the systematics of the quantum defects.

In the present paper we focus our attention on the inner-shell properties of these ions. The particular question we address is, "How do inner-shell properties vary with the removal of outer-shell electrons?" These inner-shell properties are of intrinsic fundamental interest, and they are also important as a basis for the production and detection of multicharged ions in experiments on ion-atom collisions.

The isonuclear picture is the logical one for study of this question and is generally employed in this paper. Examples of the application of the other pictures are also discussed in an effort to ascertain what further information or insights they might provide. The properties studied include inner-shell binding energies, x-ray transition energies and rates, inner-shell photoionization cross sections, and expectation values $\langle r^q \rangle$, with $q=-3$, -1, $+1$, and $+2$.

The calculations were carried out for all positive atomic ions (along with the neutrals for completeness) for $Z \leq 50$ by using Hartree-Slater central-field wave functions. The utility of these wave functions and other comments about the method of calculation are discussed in Sec. II. Section III presents our results, and the final section contains a summary and concluding remarks.

II. BRIEF DESCRIPTION OF THEORY

The calculations of energies and matrix elements presented in this work were performed by using Hartree-Slater (HS) central-field wave functions.[3-5] For a transition, the initial- and final-state wave functions were both solutions to the Schrödinger equation with the *same* potential, the HS potential for the initial state; no core relaxation was included in the calculation of transition matrix elements. In other words, the HS functions were used in this study because they are so amenable to large-scale calculation. In addition, these HS wave functions have been found to predict reasonably good results for neutral atoms[6] and for threshold phase shifts of ions.[1]

The HS formulation includes a central-field approximation to electron exchange effects;[3,4] thus, multiplet splitting and term dependence are omitted. Spin-orbit and other fine-structure effects are also omitted. Thus, our results represent the characteristics of a configuration average. Further, no correlation or channel coupling is included in our calculations. Nevertheless, none of the above omissions is expected to affect materially the systematic trends of inner-shell behavior in atomic ions.

III. RESULTS AND DISCUSSION

In atomic-collision studies, the various excitation and ionization processes are often identified by observing the produced x rays. When multicharged ions result, the question arises as to what extent the x-ray energies and intensities are influenced by the presence of outer-shell vacancies. We thus consider x-ray transitions in which inner shells are filled.

A. Orbital binding energies

First, the orbital binding energies are studied. Figure 1 shows some of the data for $1s$ to $3d$ subshells in the isoionic picture. To facilitate presentation of the data, the vertical axis represents the binding energy in Rydbergs multiplied by n^2/Z^2, where n is the principal quantum number. Since $E_{\text{hydrogenic}}=Z^2/n^2$ Ry is the binding energy of an electron in the unscreened Coulomb field of the nucleus, the vertical axis is therefore the binding energy scaled by the unscreened Coulomb value. If the binding energy were scaled to the hydrogenic value that accounts for the inner and outer screening as treated by Bethe and Salpeter,[7] all the curves would be flatter and would lie closer to unity.

The left panel in Fig. 1 refers to $z=1$, i.e., to neutral atoms. The curve for the scaled $3s$ binding energy shows a break at $Z=18$ (Ar), i.e., at a rare-gas with closed-shell structure, indicating that the structure is tighter than that of the neighbors. In addition, similar breaks at $Z=24$ (Cr) and 29 (Cu) occur because Cr with the half-filled subshell $3d^5$ and Cu with the completely filled subshell $3d^{10}$ have more tightly bound structures than their neighbors in the Periodic Table. This same effect also is seen in the behavior of the quantum defect, as discussed by Fano, Theodosiou, and Dehmer.[8] The general rise in the $3s$ scaled binding energy with Z is a consequence of the increased effective charge seen by the $3s$ electrons with increasing Z.

All of these trends in the $3s$ electrons are even more clearly seen in the $3p$ electrons. For the $3d$ electrons, the trends are also noticeable, but a new aspect is the downward trend above $Z=29$, which occurs because the $3d$ subshell in this region is the outer valence shell and fills as Z increases. Indeed, the minimum of the $3d$ curve at $Z=29$ is especially deep. This effect is also apparent in the radial expectation values, $\langle r^q \rangle$, which we shall discuss in Sec. III D.

The scaled $2s$ binding energy shows a minimum at $Z=10$ (Ne) and thereafter gradually increases with Z. Breaks at $Z=18$, 24, and 29 are still present but are scarcely discernible in Fig. 1. This observation illustrates the insularity of an inner shell from the outer-shell structure. The $2p$ binding energy behaves similarly.

The scaled $1s$ binding energy increases smoothly with Z after the minimum at $Z=2$ (He). The general proximity of the $1s$ curve to unity indicates the validity of the hydrogenic approximation as treated by Bethe and Salpeter,[7] especially with increasing Z.

For $z=2$, i.e., for singly ionized atoms, all the curves show weaker variations with Z. The effect of the filling of the $3d$ subshell is still noticeable in the binding energies for the $3s$, $3p$, and $3d$ states. The scaled binding-energy curves for the $2s$ and $2p$ subshells are smoother and have milder slopes as functions of Z, apart from the minima at $Z=11$, which correspond to $N=10$, i.e., the neonlike structure. The smooth behavior is even more clear in the $1s$ scaled binding energy.

As z increases to 3, 5, and 10, all the valence-shell effects disappear. However, a new aspect appears, i.e., minima or breaks at hydrogenic closed shells, as probably first discussed by Goudsmit and Richards.[9] These breaks occur at

$$N=n(n+1)(2n+1)/3=2,10,28,60,\ldots,$$

respectively. By $z=10$, the behavior of the binding energy is predominantly governed by the strong nuclear Coulomb field.

Thus, we observe that the energy-level structure approaches the hydrogenic behavior as z/N becomes large. Although this fact is generally known,[9] it is not widely appreciated that the approach is only asymptotic and is neither rapid nor monotonic. This recognition is a point of major significance that emerges throughout our study.

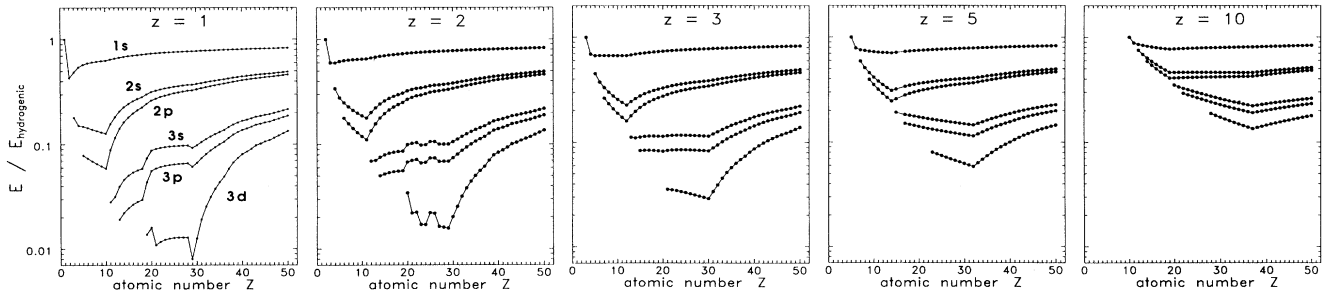

FIG. 1. Orbital binding energies for the $1s$, $2s$, $2p$, $3s$, $3p$, and $3d$ states plotted against the nuclear charge Z for fixed orders of spectrum $z=Z-N+1=1$, 2, 3, 5, and 10. The vertical axis shows the binding energies E divided by the hydrogenic value Z^2/n^2 Ry corresponding to the bare nuclear charge Z. In each panel, curves correspond to the $1s$, $2s$, $2p$, $3s$, $3p$, and $3d$ states, from top to bottom.

B. X-ray transition energies and rates

We now focus on x-ray transition energies, which are given to a good approximation by the differences between the orbital binding energies involved. To see the influence of outer-shell electrons and vacancies, it is appropriate to examine data in the isonuclear picture, as illustrated in Fig. 2. The left panels refer to Kr ($Z=36$) and the right panels to Sn ($Z=50$). For both elements,

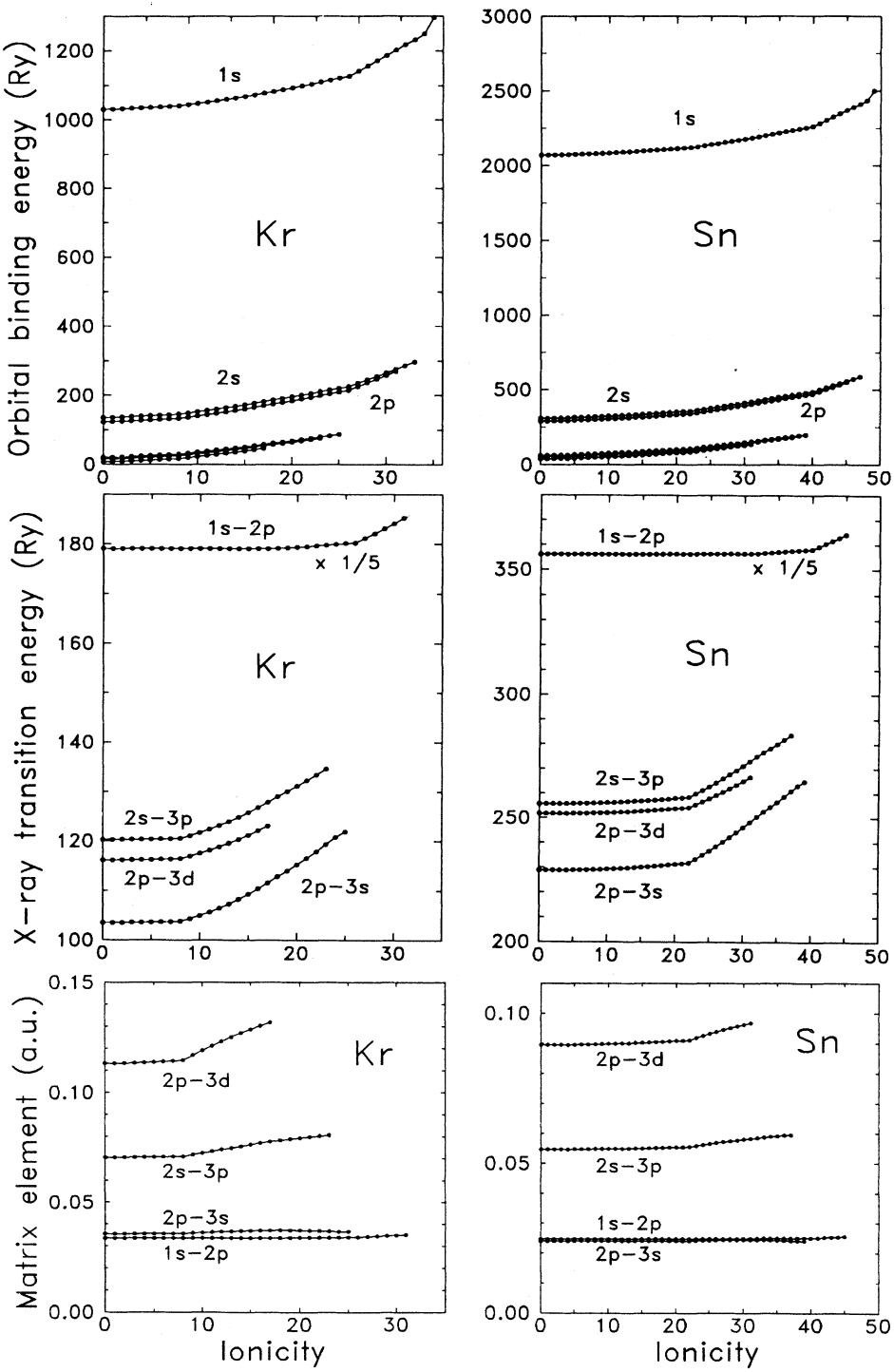

FIG. 2. Isonuclear picture for properties relevant to x-ray transitions for $Z=36$ (Kr) and 50 (Sn). Top panels: Orbital binding energies for the $1s$, $2s$, $2p$, $3s$, $3p$, and $3d$ states, plotted against the ionicity $Z-N$. The breaks in the slope of the curves indicate hydrogenic closed-shell structures, $N=10$ and 28. Middle panels: X-ray energies for the transitions $1s$-$2p$, $2s$-$3p$, $2p$-$3d$, and $2p$-$3s$, plotted against the ionicity. Bottom panels: Dipole matrix elements for the same transitions.

all the inner-shell orbital binding energies are a monotonically increasing function of the ionicity $Z-N$, as seen in the top panels of Fig. 2, which show the steadily decreasing influence of outer-shell screening. The binding energy for the $1s$ orbital, for instance, shows a slope discontinuity at $Z-N=26$ for $Z=36$ and at $Z-N=40$ for $Z=50$, both instances corresponding to $N=10$, i.e., a full L shell.

The x-ray transition energies are shown in the middle panels of Fig. 2. The transition energies for $3p$-$2s$ and $3s$-$2p$, for instance, remain virtually constant upon removal of outer-shell electrons for $0\leq Z-N\leq 8$ at $Z=36$, and for $0\leq Z-N\leq 22$ at $Z=36$. The energies show a clear slope discontinuity at $N=28$, at which value the hydrogenic M shell ($1s^2 2s^2 2p^6 3s^2 3p^6 3d^{10}$) is complete. The $2p$-$1s$ transition energy stays virtually constant upon removal of outer-shell electrons and begins to increase suddenly at $N<10$, where the L-shell structure ($1s^2 2s^2 2p^6$) begins to be affected. The trends described above were universally observed for all of the atomic ions we studied. A preliminary report[10] of the present work includes data on Rb ($Z=37$), showing the same trend.

In summary, the x-ray transition energy stays virtually constant so long as both the initial state and the final state belong to truly inner shells, because the outer-shell screening equally influences the binding energies of all the inner shells. This is readily apparent from the Gauss law of electrostatics. However, when the initial state has an open-shell structure (more precisely, when an open shell is the hydrogenic structure for highly stripped ions), a slope discontinuity occurs. Thereafter, the transition energy steadily increases as a function of z, since removal of electrons then affects the inner screening and increases the effective charge seen by the remaining electrons. These observations are consistent with experimental data on x-ray spectra as reported in Refs. 11–13, for instance, and as reviewed in Refs. 14–16.

A very recent experiment[17] that investigated the binding energies of $2s$, $3s$, and $4s$ electrons in ions of Kr admirably confirms our results. According to the discussion of the previous two paragraphs, the difference between the $2s$ and $3s$ binding energies should remain essentially constant while electrons are removed from the $n=4$ shell but should change at Kr^{9+}, where an $n=3$ electron is removed.

A comparison of our theoretical numbers with experimental results[17] (Table I) shows differences in binding energy between successive stages of ionization. A number of points emerge clearly from this table. First, the changes in binding energy of the $2s$ and $3s$ subshells remain essentially the same, i.e., the difference between $2s$ and $3s$ binding energies remains constant as outer-shell electrons are removed, both in the experiment and in our calculations. Second, these $2s$-$3s$ binding-energy differences change abruptly at Kr^{9+} as the $n=3$ shell is affected, both in the experiment and in our calculation. Next, the $4s$ binding energy changes differently than the $2s$ or $3s$ from the start, because $n=4$ electrons are removed from the start. Thus, the experimental results of Ref. 17 are clearly in complete harmony with our predictions.

In addition, Table I shows that our calculated results are in excellent agreement with both experimental results and with a calculation that includes relativistic effects.[17] Thus, we have good reason to believe that our calculated results should not only predict qualitative trends but be quantitatively accurate as well.

The rate of an x-ray transition is principally related to the transition energy and the dipole matrix elements between the initial state and the final state involved. The dipole matrix elements, shown in the bottom panels of Fig. 2, show the behavior similar to that of the transition

TABLE I. Changes in the binding energies of the $2s$, $3s$, and $4s$ electrons in the Kr isonuclear sequence upon successive removal of outermost electrons. The energies are measured in eV.

Change in ionic charge[a]	$2s$			$3s$			$4s$		
	Expt.[b]	Chen[c]	Present	Expt.[b]	Chen[c]	Present	Expt.[b]	Chen[c]	Present
0→1			12.9			12.8			11.4
1→2	14.4(3)	15.0	14.6	14.8(8)	14.5	14.3	13.0(12)	11.6	12.5
2→3	15.9(2)	15.8	15.8	16.4(4)	15.6	15.6	14.3(9)	12.4	13.3
3→4	17.3(1)	17.3	17.3	16.9(1)	16.8	16.8	14.2(5)	13.3	14.1
4→5	18.7(1)	18.7	18.2	17.9(1)	18.1	17.9	14.6(3)	13.6	14.7
5→6	20.2(1)	19.8	19.4	19.2(1)	18.7	18.8	16.1(3)	14.4	15.5
6→7	21.4(1)	21.6	21.5	20.1(1)	20.5	20.8	16.5(4)	17.9	17.0
7→8	22.2(2)	22.6	22.7	20.2(3)	20.9	21.8			
8→9	45.1(2)	45.2	45.1	38.0(3)	38.1	37.9			
9→10	45.9(3)	47.9	47.7	37.6(5)	39.2	39.4			
10→11	51.3(3)	49.0	50.1	37.3(10)	39.3	40.8			
11→12	59.4(6)	54.2	52.4			42.1			
12→13	54.0(18)	53.1	54.8			43.3			

[a]Each line in the column represents the successive removal of an electron in outermost shells. For instance, "1→2" means the change from Kr^{1+} to Kr^{2+}.

[b]Measurements by Decman and Stoeffl (Ref. 17).

[c]Calculations by Chen as cited by Decman and Stoeffl (Ref. 17). The numbers in parentheses represent uncertainties in the last digits.

energy insofar as they remain virtually constant as long as both initial *and* final states are inner shells. When inner-shell electrons are removed, the dipole matrix elements may increase rapidly. This increase in the matrix element as the inner screening is increased occurs because the effective charge increases so that the outermost subshell becomes more compact, giving greater overlap and, thus, a larger matrix element. Thus we understand the major trends of the matrix element. (As an exception, the broad weak maximum of the $2p$-$3s$ matrix element in Kr ions is not easily interpreted.)

C. Photoionization cross sections

Ample work has been presented elsewhere to document the systematics of the behavior of the photoionization cross section of inner shells;[18,19] for completeness, however, we present our results for the $2p$ and $3s$ subshells in the Zn isonuclear sequence in Figs. 3(a) and 3(b), respectively. Although calculations were performed for each stage of ionization, the cross section for $2p$ photoionization remains on the same curve from the neutral atom to Zn^{20+}; only at higher stages of ionization, as the $2p$ subshell is affected, is there a change. Similarly, for the $3s$ subshell the change occurs at Zn^{3+}, where a third electron is removed, showing that it is the shell (i.e., the principal quantum number) that is important. As electrons from the same shell as the photoelectron are removed, the cross section per electron steadily increases. This increase occurs because removing electrons from the same shell obviously decreases the screening, thereby increasing the effective charge seen by the photoelectron. Since the cross section near threshold increases with Z, such an increase is observed.

The matrix element for an inner-shell ionization receives contributions entirely from the inner region owing to the extent of the inner-shell wave function. Even though the normalization of the final continuum wave function is determined by the potential at large r, removal of outer electrons still has no substantial effect on the continuum wave function in the inner region. Furthermore, this phenomenon also appears in more advanced theoretical treatments, e.g., relativistic random-phase approximation (RRPA).[20]

D. Expectation values of powers of r

The expectation values of powers of the electron radial coordinate r^q are sensitive to changes of the atomic potential in the small-r ($q<0$) and large-r ($q>0$) regions to which an orbital extends. Thus, changes in the atomic potential, e.g., by stripping outer electrons, will be noticed for some powers of q ($q>0$) and not noticed for others ($q<0$). At the same time, the various powers of r are directly related to specific and diverse physical properties of ions and atoms, and reflect the dependence on changes in the atomic potential due to changes in the outer shell's degree of occupation by electrons. The following examples of powers of r are examined here in more detail.

$\langle r \rangle$ gives the average size of an electron's probability density (i.e., the size of the electron cloud);[7] $\langle r^2 \rangle$ is proportional to the atomic electric quadrupole moment and

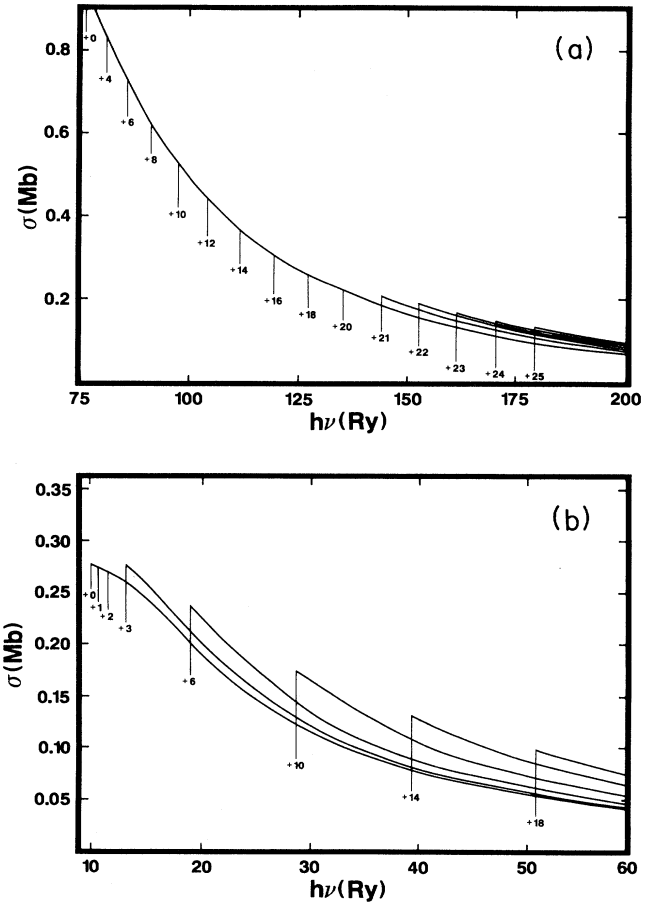

FIG. 3. Photoionization cross section per electron of the $2p$ [panel (a)] and $3s$ [panel (b)] subshells for the full Zn ($Z=30$) isonuclear sequence. The vertical lines indicate the thresholds for the given stage of ionization, $z-1$.

is proportional to the diamagnetic susceptibility[7] and approximately to the total inelastic-scattering cross section;[21] $\langle r^{-1} \rangle$ is proportional to the energy of the electron's interaction with the nucleus, but it is also an appropriate index of the total energy, especially with increasing atomic number Z; and $\langle r^{-3} \rangle$ is proportional to the spin-orbit interaction effect on the electronic energy.[8]

In the pure hydrogenic case, i.e., when only one electron is present, all of these expectation values are known exactly and are given analytically[7,22] (for the orbitals for which they have a finite or meaningful value). Their significance in the nonhydrogenic cases arises because their departure from the corresponding hydrogenic value is a direct consequence of the electron-electron interactions. Thus, a more meaningful graphic representation of most of these quantities shows them relative to their respective hydrogenic values.[7,22] A systematic study of these reduced values of $\langle r^q \rangle$ thus yields an excellent description of the systematic behavior of at least some of the electron-electron interactions as they are affected by changes in the atomic or ionic potential.

Figure 4 shows the renormalized expectation values of

$\langle r^q \rangle$, $q = +1$, $+2$, -1, and -3 for the $n = 1$, 2, and 3 orbitals in the isonuclear case. The hydrogenic values were calculated for a charge equal to the bare-nucleus value Z. The order of the curves is $1s$, $2s$, $2p$, $3s$, $3p$, and $3d$, from the bottom of graphs for positive q, and inversely for negative q. The ns orbitals have infinite $\langle r^{-3} \rangle$ and are not shown in the graph. Figure 4 shows that the $\langle r \rangle$ and $\langle r^2 \rangle$ of the inner shells ($n = 1$ and 2) are practically unchanged while the electrons from the $n = 4$ and 3 shells (in that order) are being stripped off, but that the $n = 2$ orbitals contract suddenly and significantly when the $n = 2$ shell is opened and the inner screening is reduced. This behavior occurs because the $1s$, $2s$, and $2p$ orbitals in these ions are very close to the nucleus. On the other hand, the orbitals $3s$, $3p$, and $3d$ are successively more physically extended and are very significantly affected by changes in the outermost shells, because these changes reduce their inner screening and make them more compact.

The rather surprising result is the small but perceptible variation of $\langle r^{-1} \rangle$ and $\langle r^{-3} \rangle$ for $2s$ and $2p$ from about $z = 10$ to 20. Since these powers emphasize the portions of the wave functions near the origin, one would expect that they should have the least possible change with outer-shell stripping. Instead, as soon as the $3d$ subshell is opened, a noticeable effect on $2s$ and $2p$ is taking place, more so than for the positive powers of r, which emphasize the outer region. Because the full nuclear charge Z rather than the effective charge Z_{eff} is used to calculate the hydrogenic values, the changes in slope cannot be at-

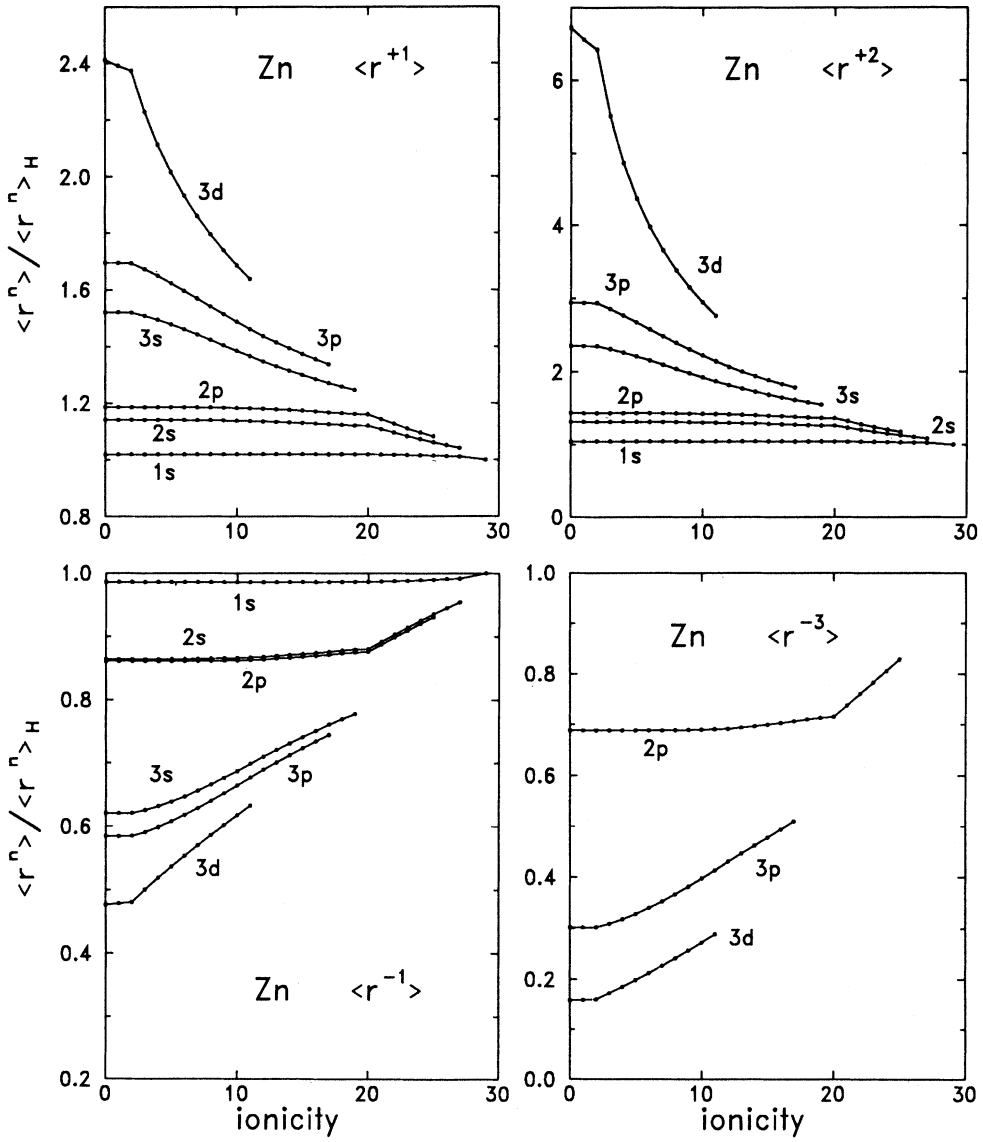

FIG. 4. The expectation values of $\langle r^q \rangle$, with $q = -3$, -1, 1, 2, for the Zn ($Z = 30$) isonuclear sequence. The vertical axis represents $\langle r^q \rangle$ divided by the hydrogenic value corresponding to the bare charge Z.

tributed to choices of Z_{eff}. This behavior indicates that $\langle r^{-1} \rangle$ and $\langle r^{-3} \rangle$ are very sensitive to very slight changes of electron density near the nucleus, while $\langle r \rangle$ and $\langle r^2 \rangle$ appear to be far less sensitive to small changes in inner screening.

IV. FINAL REMARKS

Inner-shell properties of atomic ions, including binding energies, x-ray transition energies and rates, photoionization cross sections, and expectation values of various electron radial coordinates, have been studied with Kr and Sn as examples. A major result is that all of these properties (except binding energies) remain essentially constant along an isonuclear sequence when outer electrons are removed. This was explained by using Gauss's law, which shows that a spherical distribution of charge exerts no forces inside the distribution but changes the potential by a constant. Thus, even though inner-shell binding energies change considerably along a series, their differences (x-ray transition energies) remain constant. Some very small variations are, however, seen in $\langle r^{-1} \rangle$ and $\langle r^{-3} \rangle$, much more than in $\langle r \rangle$ and $\langle r^2 \rangle$. We have not fully explained the origin of this observation.

It was also found that when inner shells become outer shells, i.e., when electrons with the same principal quantum number as the electron being considered are removed, the properties change. This change decreases the inner screening, increases binding energies, and makes the remaining electron wave functions more compact, thus affecting all of the inner-shell properties as described.

Finally, a framework has been given for the evaluation and interpolation of inner-shell properties of atomic ions. As experimental data are accumulated, study of the isonuclear sequences will be the most useful means of both checking the data and deriving the physical information concerning the interplay between nuclear and noncentral forces.

ACKNOWLEDGMENTS

We thank C. Lewis Cocke, Jr. and Yohko Awaya for pointing out the literature on experimental x-ray spectra of atomic ions. This work was supported in part by the U.S. Department of Energy, Assistant Secretary for Energy Research, Office of Health and Environmental Research, under Contract No. W-31-109-Eng-38, and in part by the U.S. Army Research Office.

[1]C. E. Theodosiou, S. T. Manson, and M. Inokuti, Phys. Rev. A **34**, 943 (1986).

[2]C. E. Theodosiou, M. Inokuti, and S. T. Manson, At. Data Nucl. Data Tables **35**, 473 (1986).

[3]F. Herman and S. Skillman, *Atomic Structure Calculations* (Prentice-Hall, Engelwood Cliffs, NJ, 1963).

[4]J. P. Desclaux, Comput. Phys. Commun. **1**, 216 (1969).

[5]S. T. Manson, Phys. Rev. **182**, 971 (1969).

[6]S. T. Manson and J. E. Purcell, Phys. Rev. A **15**, 1319 (1977), and references therein.

[7]H. A. Bethe and E. E. Salpeter, *Quantum Mechanics of One- and Two-Electron Atoms* (Springer, New York, 1957).

[8]U. Fano, C. E. Theodosiou, and J. L. Dehmer, Rev. Mod. Phys. **48**, 49 (1976).

[9]S. A. Goudsmit and P. I. Richards, Proc. Natl. Acad. Sci. U.S.A. **51**, 664 (1964).

[10]S. T. Manson, M. Inokuti, and C. E. Theodosiou, in *Dynamic Processes of Highly Charged Ions,* Proceedings of an International Seminar, Fuji, Japan, 1986, edited by T. Watanabe *et al.* (Institute of Physical and Chemical Research, Wakoshi, Japan, 1986), p. 39.

[11]K. W. Hill, B. L. Doyle, S. M. Shafroth, D. H. Madison, and R. L. Deslattes, Phys. Rev. A **13**, 1334 (1976).

[12]Y. Awaya, M. Akiba, T. Katou, H. Kumagai, Y. Tendow, K. Izumo, T. Takahashi, A. Hashizume, M. Okano, and T. Hamada, Phys. Lett. **61A**, 111 (1977).

[13]C. Schmiedekamp, B. L. Doyle, T. J. Gay, R. K. Gardner, K. A. Jamison, and P. Richard, Phys. Rev. A **18**, 1892 (1978).

[14]R. L. Kauffmann and P. Richard, in *Methods of Experimental Physics,* edited by D. Williams (Academic, New York, 1976), Vol. 13, Part A, p. 148.

[15]F. Hopkins, in *Methods of Experimental Physics,* edited by P. Richard (Academic, New York, 1980), Vol. 17, p. 355.

[16]Y. Awaya, in *Electronic and Atomic Collisions, Proceedings of the Tenth International Conference on the Physics of Electronic and Atomic Collisions, Kyoto, 1979, Invited Papers and Progress Reports,* edited by N. Oda and K. Takayanagi (North-Holland, Amsterdam, 1980), p. 325.

[17]D. J. Decman and W. Stoeffl, Phys. Rev. Lett. **64**, 2767 (1990).

[18]S. T. Manson and R. F. Reilman, Astrophys. J. Suppl. **40**, 815 (1979), and references therein.

[19]S. T. Manson, in *Electronic and Atomic Collisions,* edited by A. Dalgarno, R. S. Freund, P. M. Koch, M. S. Lubell, and T. B. Lucatorto (American Institute of Physics, New York, 1990), p. 189.

[20]G. Nasreen and S. T. Manson, Phys. Rev. A **40**, 6091 (1989).

[21]M. Inokuti, Rev. Mod. Phys. **43**, 297 (1971).

[22]K. Bockasten, Phys. Rev. A **9**, 1087 (1974).